Prediction of Synthesis of 2D Metal Carbides and Nitrides (MXenes) and Their Precursors with Positive and Unlabeled Machine Learning

Terek Li
999825961

MSE-1065 Final Report

Abstract

This project uses open source dataset and positive and unlabelled machine learning technique to predict synthesizability of MXene and MAX precursor. Detailed hyper-parameter tuning is carried out to generate a model with true positive rate greater than 0.9. The finalized model is then used to predict that 155 unlabelled MAX and 19 unlabelled MXene could be synthesized. Analysis of the model output suggests unique result regarding synthesizability of MXene that is not reported in literature. A further analysis to match MXene with respective precursor suggest that only 11 MXene could be synthesized due to the lack of synthesizable MAX precursor. Overall, this project could push forward the discovery of new generation of MXene, which would greatly expand material selection freedom for high performance applications.

1 Introduction

MXene is a new family of two-dimensional (2D) material that was first discovered in 2011 by Naguib et al. using Density Functional Theory (DFT), they standout against other 2D material for their excellent electrochemical properties and a wide range of other properties such as tunable optoelectronic properties [1], flame-retardancy [2–4], unique electromagnetic-interference shielding mechanism [2, 5, 6], and finally ability to easily disperse and stabilize in water medium [7, 8]. MXene is produced from MAX phase precursor with chemical formula $M_{n+1}AX_n$ where $n = 1, 2$ or 3. M is an early-transition metal such as titanium, A is mostly from Group 13 or 14 of periodic table such as aluminum, and X is either carbon or nitrogen [9] (Figure 1). MAX phases form layered hexagonal structures (space group $P6_3/mmc$) of early transitional metal carbides with two formula units per cell bond together by the A element. The removal of A group layer from MAX phases result in 2D $M_{n+1}X_n$ layer known as MXene (Figure 2), named to denote the loss of A group and to emphasize its morphology and geometrical similarities to graphene [9]. After etching the end groups of MX layers are satisfied by termination elements such as OH and F, and these are often denoted with T_x.

The vast properties of MXene enabled it to be used for a wide range of applications including a key enabler for various components of Internet of Things (IoT). MXene have been incorporated into porous films and electrospun fibers as contact material for triboelectric-nano-generator (TENG) to convert contact force into alternative current [10]. It could then be printed as supercapacitors and batteries to power a wide selection of environmental, bio and mechanical sensors with high signal to noise ratio. To complete the operation circuit for IoT, spray coated MXene could be used as radio-frequency antennas for wireless communications for up to eight meters [11]. Furthermore, unique optoelectronic properties of MXene enabled it to be selectively etched to transmit ~90 % of the light in the visible-to-infrared range while maintaining metallic conductivity [12], expanding MXene's potential applications into the wearable and smart electronic territory. The integration of additive manufacturing with unique functionalities of MXene could further accelerate the growth of MXene's real world applications, allowing for all-printed electronics using MXene [13].

Although currently more than 30 MXenes have been successfully synthesized [14, 15], research interest in this field is still heavily focused on the original $Ti_3C_2T_x$ that was first discovered in 2011 due to $Ti_3C_2T_x$ having one of the highest electrical performances and well understood synthesizing method. However, $Ti_3C_2T_X$ has its own short comings such as susceptible to oxidation [16] and restacking of MXene flakes which reduces ion transport mobility [17]. These severely limited MXene's implementation in real world applications and opened incentive in developing more high performance MXene species. The synthesis of MXene is a time consuming and complicated process, therefore, using machine learning strategy to predict potential MAX precursor and corresponding 2D MXene is a promising strategy. In 2018 Frey et al. demonstrated prediction of MXene and their precursor with positive and unlabeled machine learning [18]. This project aims to carry out similar modelling work but using a condensed dataset to reduce computational

time. The result gained from this work in some part contradict Frey et al.'s result, but largely compliment it by providing unique insight into synthesizability of different MXene.

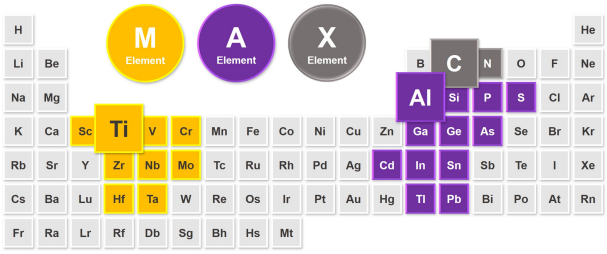

Figure 1: Chemical composition of MAX phase precursor with formula $M_{n+1}AX_n$ where $n = 1, 2$or 3. MXene is produced by removing the A layer from MAX.

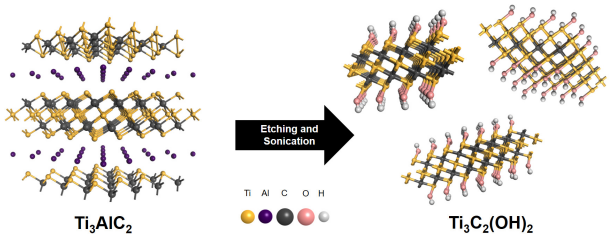

Figure 2: Atomic model of MAX precursor and MXene. The weakly bonded A layer is first etched away, the MXene layers are then exfoliated by sonication or vigorous hand shaking to form a stable dispersion in water.

1.1 Literature Review

To produce MXene from MAX precursor, chemical etching is often required to break the bonds between MX and A layers as bonding strength is too strong to be broken by mechanical shearing [19]. Figure 3 illustrate the etching and exfoliation process of $Ti_3C_2T_x$ MXene from Ti_3AlC_2 MAX. The A group atoms (Al) are weakly bonded and are the most reactive species, allowing for room temperature extraction with hydrofluoric acid (HF). After etching, large ions such as Li^+ can be inserted between MXene layers to intercalate and increase interlayer spacing, which allows for full exfoliation into single-layer MXene flakes by sonication. This general synthesis method is not only limited to $Ti_3C_2T_x$ but also applies to most MXene.

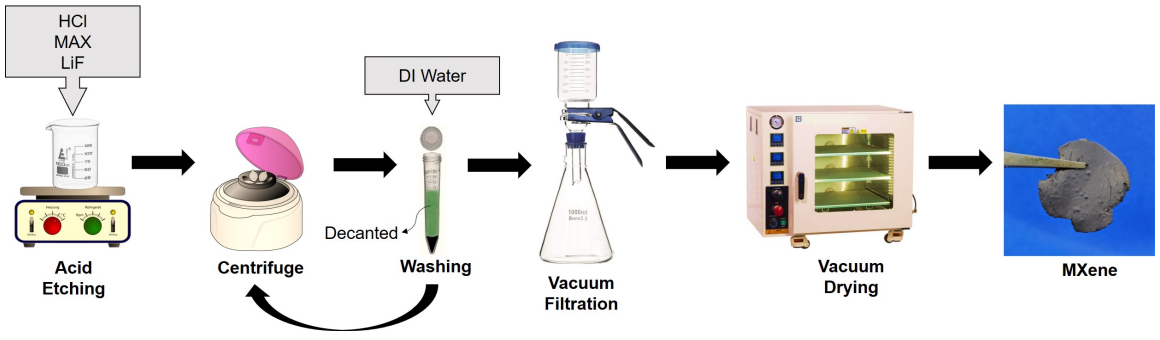

Figure 3: Etching of MAX to MXene. LiF is first dissolved in HCl to form in-situ HF, MAX precursor is added to etch for 24 to 48 hr at room temperature. After first round of centrifuge the supernatant is a dark green solution. The sediment is receptively washed until reaching pH of 6 after which the solution is filtered and dried to obtain a self standing MXene cake.

Experimentally synthesis of new generation of MXene is enormously time consuming and whether

Table 1: Experimentally synthesized MXene. Summarized from [9, 18, 22].

Ti_2C	$TiNbC$	Ti_3CN_x	Ta_4C_3	Ti_3C_2	Hf_3C_2
Nb_2C	V_2C	Mo_2C	Nb_4C_3	Ti_4N_3	Zr_3C_2
Sc_2C	Ti_2N	Zr_2C	Zr_2N	Hf_2C	Hf_2N
Ta_2C	Cr_2C	Cr_2N			

a theoretical MXene can be successfully produced is not guaranteed. Although Density Functional Theory can shed some light to suggest potential existence of new generation MXene, it still requires Design of Experiment to determine proper processing parameters and to confirm the result. Table 1 summarizes the existing MXene that has already been experimentally synthesized. Indeed, there is great interest to use computation to accelerate the prediction of possible MXene.

Machine learning (ML) is a powerful tool for determining properties and processing parameters of next generation material. Previously ML has been used to predict the stability [20] and band gap of MXene [21]. The difficulty is how to develop a representative and accurate model using a small quantity of data-set. Algorithms such as random forest, logistic repression, support vector machine (SVM), Gaussian process (GPR), kirnel ridge (KRR) and k-nearest neighbors (KNN) have all been used for this purpose. Among these techniques, decision-tree classifier is considered a promising and reliable method for positive and unlabelled (PU) machine learning to train a limited data-set. Furthermore, Frey et al. compared SVM agaisnt decision tree and concluded that both are highly suitable for PU ML to predict synthesis of MXene.

1.2 Positive and Unlabelled Machine Learning (PU ML)

Using ML to predict properties and process ability of advanced material is often faced with the challenge of having insufficient and unreliable data labels. For example, we could have 1000 samples but only 100 of them have reliable positive label, and the remaining 900 are either unreliable negative or unlabeled. Therefore there could be some positive samples mixed in this unreliable sample pool. PU learning is an excellent strategy to address this problem by using a semi-supervised binary classification method to recover labels from the unknown sample pool. PU learning does this by a strategy known as PU bagging to learn from the reliable positive label pool and applying what it has learned to relabel the unknown cases.

PU bagging randomly picks data from the unlabelled pool and combine with the entire labelled pool to create a training set. The labelled sample is tagged as 1 whereas the unlabelled sample is tagged as 0. This training set is referred to as the "bag" and can be processed to generate a classifier which output a probability score for each unlabelled sample outside of the training set which is also referred to as out-of-bag samples (OOB). This process can be repeated to calculate average OOB scores. Figure 4 illustrate PU bagging procedure. The Scikit learn library of Python has build in PU bagging function: *sklearn.ensemble.BaggingClassifier* to carry out the calculation. The trained model from each bag is finally combined together to generate the final trianed model.

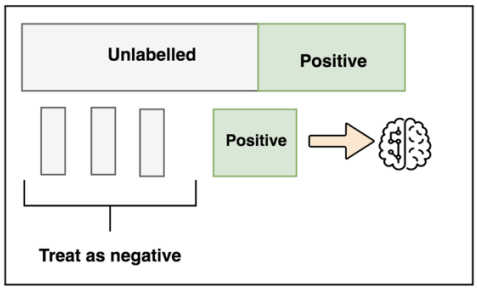

Figure 4: Illustration of PU bagging procedure.
Taken from `fritz.ai`

2 Method

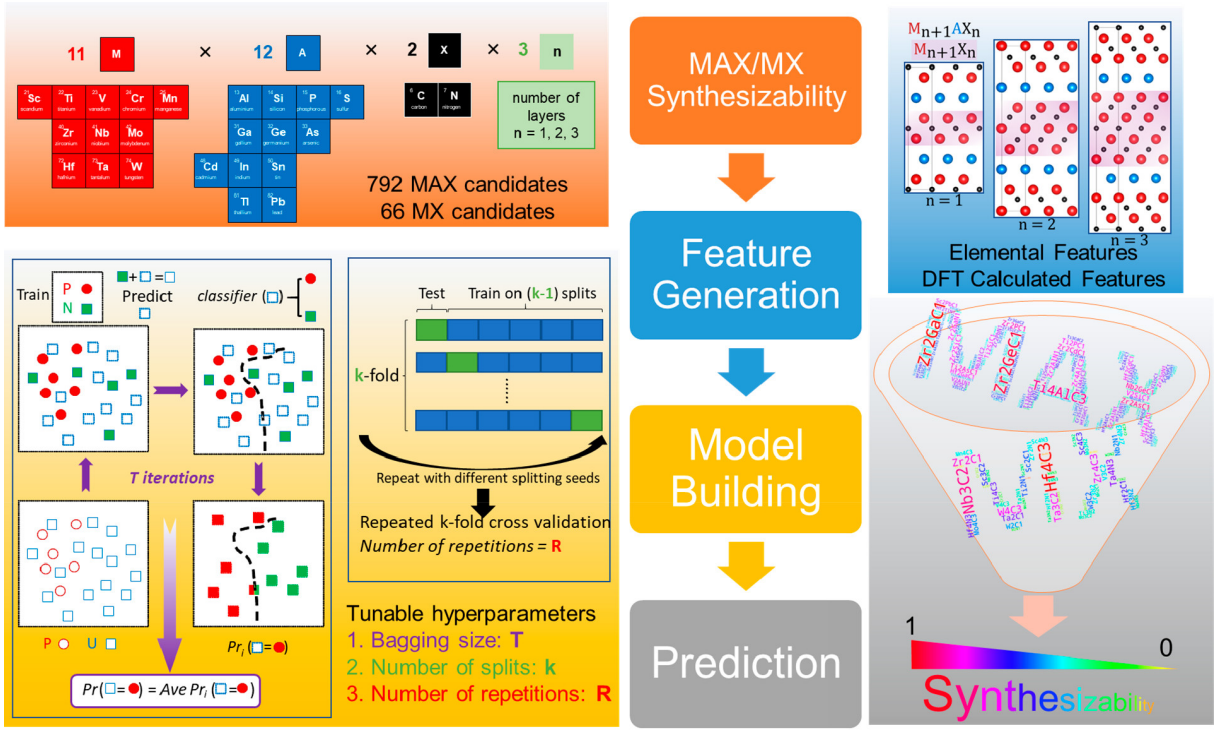

Figure 5: Schematic of the computational workflow of the PU learning process as used by Frey et al. This project used an adapted workflow based on this.

The modelling workflow is depicted in Figure 5 as outlined by Frey et al. but with my own modifications. The dataset is obtained from *pumml* on Github. *Pumml* is an open source Python library that performs positive and unlabeled material machine learning (hence the name *pumml*) to classify materials when data is either incomplete or when examples of positive data is insufficient. *Pumml* offers a test dataset consisting of 66 entries of MXene phase and 792 entries of MAX phase. Only single *M* element is considered in order to reduce computational complexity. Of these entries, 10 entries of MXene and 63 entries of MAX phase are labeled positive (already successfully synthesized). Therefore, a fraction over 10 % of overall data are labelled positive, and the rest are unlabelled, making this *pumml* work a semi-supervised machine learning approach.

pumml uses decision tree classifier in conjunction with PU bagging technique to predict a synthesis score for each input entries. A higher score indicates a greater likely hood of successful

Table 2: Summary of features used for modelling as provided by *pumml*.

Model features	
n	$M_{n+1}X_n$
a	in-plane lattice constant
E_{form}	formation energy
E_{coh}	cohesive energy

synthesis. The three key hyper-parameters, T, k and R (discussed later in this section) are tuned manually to maximize model accuracy.

Frey et al.'s work considered a wealth of structural, thermodynamic, electronic structure, and elemental data input features for their model. In total 80 features were considered, and PU bagging was implemented with a decision tree classifier to determine the 29 statistically important features. The dataset used for this project only consist of 4 features as shown in Table 2. However, these features represent four of the highest importance as confirmed by feature selection result from Frey et al. Using only the most important feature for model prediction can to some extent avoid over fitting as well as reduce computational time, which is highly desirable for this project.

The sample space is represented by randomly distributed positively labelled data (red square in Figure 5) and unlabelled blue square data. Some of the unlabelled samples are first randomly labelled as negative (green square), a decision tree is then constructed based on these data to classify the remaining labelled sample as either positive (1) or negative (0). These process are repeated for T times where T is the number of bagging size. In each iteration a new set of sample are forced to be negatively labelled for the classifier. The synthesizability score of an unlabelled sample is calculated as the average of the predictive score from all the decision tree classifiers that do not contain that sample. A score of greater than 0.5 is labelled as positive and vise versa.

The model is trained by T iterations and repeated R times with the data split into k number of folds. Upper limit for k value is the number of positively labelled entries in respective dataset. Hyper-parameter tuning is performed based on these three parameters. Frey et al. defined a TPR term as the validation metric, which is the percentage of correctly classified positive samples that are pre-labelled (Equation 1).

$$TPR = \frac{1}{R}\sum_{r=1}^{R}\frac{1}{K}\sum_{k=1}^{K}TPR_{k,r} \tag{1}$$

3 Results and Discussion

A correlation heat-map is a colorized matrix displaying the correlation coefficients between input features, a higher coefficient indicates stronger correlation and vise versa. It can effectively summarize the data. The correlation matrix of MAX and MXene is shown in Figure 6. Both MAX and MXene demonstrated weak interaction between in-plane lattice constant (a) and cohesive energy (E_{coh}). Since cohesive energy is the energy gained by arranging the atoms in a crystalline state, this indicates that changes in lattice parameter due to intercalation of larger ions (such as Li^+ from MILD) has minimal interference on cohesive energy. Strongest correlation for both MAX and MXene is between formation energy (E_{form}) and PU label. This is in agreement with Frey et al.'s feature selection result which indicated strong dependency of synthesizability from formation energy.

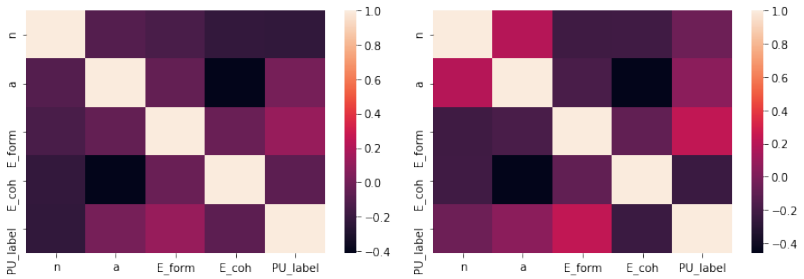

(a) (b)

Figure 6: Feature correlation matrix for MAX (left) and MXene (right).

3.1 Hyper-parameter Tuning

The *pumml* library does not contain build in hyper-parameter tuning function. Therefore, a detailed and exhausive tuning process is carried out manually by varying the three selected parameters: number of split (k), bagging size (T), and number of repetitions (R). In every set of test two parameters are fixed while one is varied incrementally between small and large values. Frey et al.'s result indicates that normalization of the dataset with respect to the number of atoms can effectively improve TPR between 0.02 to 0.1 depending on how the hyper-parameters are tuned. To validate this conclusion using the condensed dataset from *pumml*, hyper-parameter tuning is carried out twice for each set of tests, once using the raw dataset and once more using the normalized data. TPR result for raw data is shown in blue and normalized data result is shown in orange (Figure 7).

Opposite to Frey et al.'s finding, the normalized data consistently performed less ideally than raw data, with a approximately 0.4 reduction in TPR. A hypothesis for this contradiction is that the termination group of MXene is neglected in Frey et al.'s model. For example, the most widely researched MXene Ti_3C_2 rarely exist in pristine form, but always has either $(OH)_2$ or F_2 to neutralize charges [23]. These termination atoms greatly influence the total atom counts and therefore affect how the data is normalized. Frey et al.'s database consisted a wealth of input features such as energy per atom (E_{pa}) and Bader charges (e_M) which could to some extend offset the lack of termination group. However, the condensed dataset used for this project does not take the above two features into consideration, thus received polar results. Since raw data consistently out performed atom-normalized data, therefore the raw data will be used for all model training and predictions.

The number of split, k value, is ranged from 2 to the number of positively labeled samples as discussed in Section 2. For the MAX model the highest TPR of 0.92 is achieved at $k = 2$ (Figure 7a), with decreasing TPR as k values increased. However, the TPR across different split value are consistently higher than Frey et al.'s result. Cross validation of MXene dataset is challenging due to the lack of positively labeled data points (10 in total). Figure 7d shows that for MXene the best performance of 0.91 is reached at $k = 8$. In comparison, this is also very close to where MAX dataset reached highest TPR. At $R = 200$ and $T = 200$ the optimal k value is between 2 and 10.

The bagging size, T, determines the number of base models generated for the ensemble averaging. For MAX phases there is very small fluctuation in TPR across 1000 T values, with the highest TPR of 0.89 at $T = 100$ and $T = 200$, and the lowest TPR of 0.87 at $T = 1000$ (Figure 7b). This trend is more obvious for MXene as there is almost no variation across all T values (Figure 7e). The modelling result shows weak dependency on bagging size. Therefore, a smaller bagging size of less than or equal to 200 could be implemented to reduce computational time while maximising TPR for MAX phase.

The number of repetition, R, is tested at $k = 10$ and $T = 200$. For MAX phases the TPR consis-

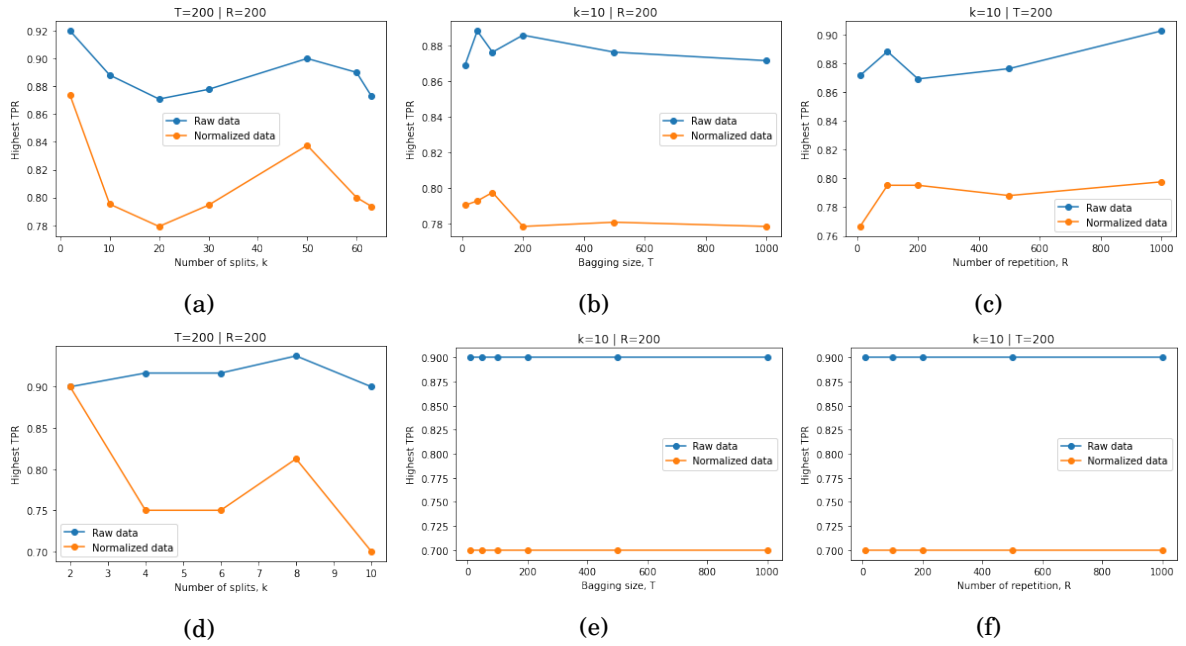

Figure 7: Hyper-parameter tuning using raw and normalized data. Top row (a), (b) and (c) correspond to MAX phase. Bottom row (d), (e) and (f) correspond to MXene. Model performance is measured by maximum TPR tested as a function of number of split (k), bagging size (T) and number of repetition (R).

tently increased gradually after $R = 200$ to a maximum value of 0.95 at $R = 1000$. This is a 10 % increase from the lowest TPR of 0.87 at $R = 200$ (Figure 7c). As for MXene, in-dependency of TPR on repetition is also observed. The TPR is consistently at 0.9 across all R values. Therefore, a higher repetition is desirable for model training, but at the cost of increased computational time.

Summarizing the above analysis, TPR is maximized with number of split (k) of close to 10, A bagging size (T) of 200 and repeating by 1000 times (R). These are the result from manual hyper-parameter tuning, and will be used for model prediction and validation for both MAX and MXene.

3.2 Model Prediction

Both MAX and MXene are fitted to the model using the optimized hyper-parameters to determine the synthesizability score. A lower score indicates less probability for the material to be synthesized and vise versa. A score of greater than 0.5 can be classified as synthesizable, and a score of less than 0.5 is not synthesizable [18]. 155 of the 729 unlabelled MAX phases and 19 of the 56 unlabelled MXene phases are predicted as synthesizable. Since research interest is focused on MXene but not MAX, therefore the synthesizability result for MAX is only briefly discussed here. Figure 8a shows the percentage distribution of synthesizable MAX phases arranged by the M element, which has significant influences on the electronic and physical properties of MAX [19]. Overall M element has very little discrepancy with respect to synthesizability.

The synthesizable MAX phases are distributed relatively uniformly along the 11 M elements, with approximately 9 to 10 % accounting for each. Interestingly, MAX phases composed of Ti as M element has the fewest predicted compounds, however, this is the group of MXene that is receiving the most research interest. Furthermore, Figure 8b shows that the predicted elements is also distributed uniformly among the three different n values. n value is an important parameter for MXene properties has it affects the mechanical strength of MXene [24]. This analysis concluded that there are equal quantity of the potentially synthesizable MAX phases precursor among different M element and n value. Frey et al.'s result indicated that the M element Zr has

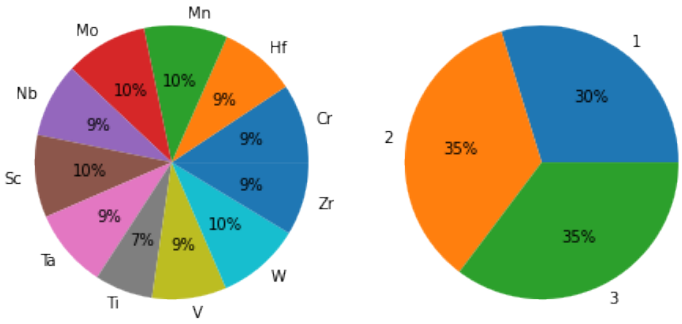

(a) (b)

Figure 8: Distribution synthesizable MAX phases arranged by M element (left) and n (right).

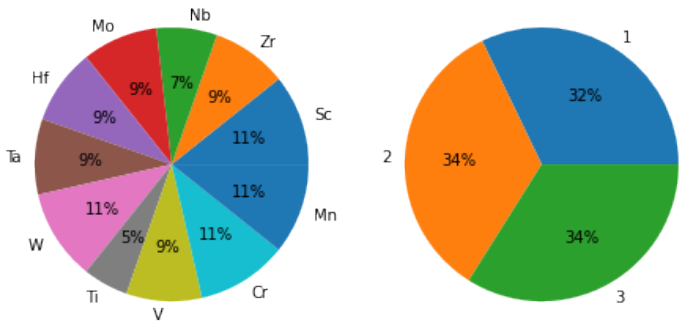

(a) (b)

Figure 9: Distribution synthesizable MXene arranged by M element (left) and n (right).

the highest synthesizability score while W has lowest. Result from this project does not contradict with Frey et al.'s findings, but rather complement it by demonstrating that a lower synthesizability score does not indicate fewer synthesizable MAX precursor.

The distribution of synthesizable MXene follows the same trend as that of MAX phase precursor. Percentage distribution of synthesizable MXene arranged by the M element shows even distribution of approximately 10 % for each M element (Figure 9a). Figure 8b shows that the predicted elements is also distributed uniformly among the three different n values. The number of MAX and MXene with different n values are equally distributed in the original dataset, with 264 MAX entries and 22 MXene entries for each n value. The same even distribution is also observed for M element, with 72 MAX entries and 6 MXene entries for each unique M element. Overall, it can be concluded that there are equal number of synthesizable MXene and MAX with respect to different M element and n value.

To further explore the synthesizability of MXene, the synthesis score of synthesizable MXene is arranged in the same color by the M element as shown in Figure 10. We can observe that there is no distinctive pattern between different M element on the synthesis score. For example, W_2C, W_3C, and W_4C are scattered along the synthesis score range. In fact, all M elements have corresponding MXene in both low and high synthesis score range. It is to ignore the result that almost all of the predicted MXene have Carbon as the X element with the exception of Ti_3N and V_4N, making $X = C$ account for 89 % of the synthesizable MXene. This agrees with Frey et al.'s findings which also demonstrated a higher synthesis score for $X = C$ MXene. Most importantly, the most significant trend from Figure 10 is that MXene with larger n values always have higher synthesis score than that with lower n value, a pattern that was not reported by Frey et al. All

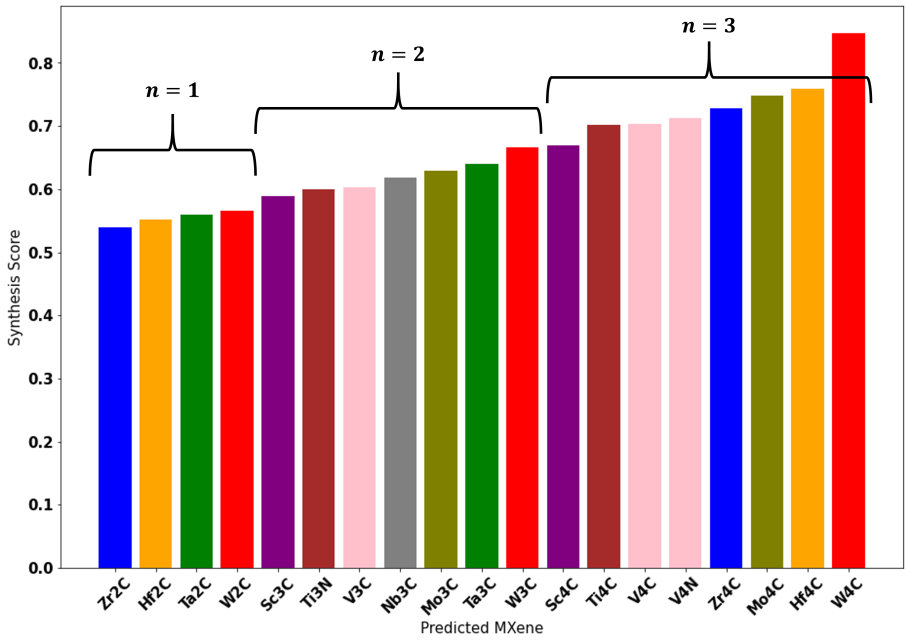

Figure 10: Synthesis score of synthesizable MXene arranged in ascending order. MXene with the same M element is labelled in the same color.

the synthesizable MXene can be categorized into three bins according to n value. The first bin with $n = 1$ has synthesis score of less than 0.55. The second bin with $n = 2$ has synthesis score between 0.55 to 0.65, and the final bin with $n = 3$ has score between 0.65 to 0.85. Therefore, we can conclude that difference in M element does not affect the likelihood to successfully synthesis MXene, whereas $X = C$ MXene with larger n values tend to have a higher probability of being synthesized.

Overall the predicted synthesizable list of MXene largely overlaps with Frey et al.'s work. 19 MXene is deemed synthesizable from this model, whereas Frey et al. identified 18 MXenes. 5 synthesizable MXenes from Frey et al.'s work is not outputted from this model, and 6 MXenes from this model was not outputted from Frey et al.'s model. These results are summarized in Table 3. Furthermore, two of the experimentally synthesized MXene from Table 1, namely Hf_2C and Ta_2C, are unlabelled but predicted as synthesizable by my model. This further proves the robustness of this trained model.

Different MXene has to be synthesized from corresponding MAX precursor according to the formula $M_{n+1}AX_n$, a MXene can only be synthesized if its MAX precursor can also be synthesized. The predicted synthesizable MXene shown in Table 3 is used to determine the number of synthesizable MAX precursor respectively, and the result is summarized in Figure 11. Out of the 19 synthesizable MXene, only 10 of them have a synthesizable MAX precursor. Therefore, these are the MXene that can be truly synthesized, whereas the remaining 9 MXene could not be synthesized although the model outputs a synthesis score of greater than 0.5. It can be observed that there is no distinctive correlation between available MAX precursor with respect to synthesis score of MXene. For example, $n = 1$ MXene with low synthesis score such as Zr_2C, Hf_2C and Ta_2C, and $n = 3$ MXene such as Ti_4C and Zr_4C with high synthesis score all have more than 5 available MAX precursor. However, MXene with $n = 2$ tend to have the list number of available MAX precursor.

Table 3: Summary of MXene output from this model and that from Frey et al.'s model.

In both model	Only in Frey et al's model	Only in this model
Zr_2C, Hf_2C	Ta_4N_3, Ti_2N	W_2C, Ti_3N_2
Ta_2C, Sc_3C_2	Hf_4N_3, Sc_2C	V_3C_2, Mo_3C_2
V_3C_2, Nb_3C_2	Nb_2N	V_3C_3, V_4N_3
Mo_3C_2, Ta_3C_2		
W_3C_2, Sc_4C_3		
Ti_4C_3, V_4C_3		
V_4N_3, Zr_4C_3		
Mo_4C_3, Hf_4C_3, W_4C_3		

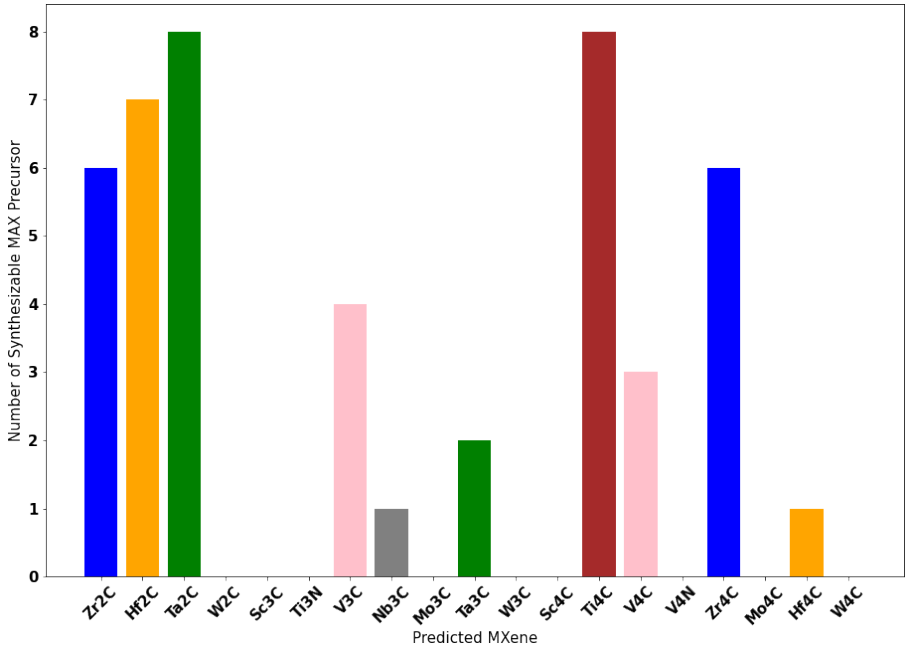

Figure 11: Synthesizable MXene arranged in the same order as Figure 10 showing corresponding number of synthesizable MAX precursor.

4 Summary and Future Work

In this project open source database and python library is used for positive and unlabelled machine learning to predict synthesis-ability of MXene and MAX precursor. The general workflow follows that proposed by Frey et al. but with my own unique alterations. First, this project demonstrates via detailed hyper-parameter tuning that normalization of dataset with respect to the number of atoms does not provide higher TPR when the number of input features are limited. Second, model output from this project gives special insight into synthesizability of MXene and MAX. Specifically, difference in n value and M element does not influence the overall quantity of synthesizable MXene and MAX, but a higher n values does increase the synthesizing probability of corresponding MXene. Finally, not all predicted synthesizable MXene can indeed be synthesized due to the lack of synthesizable MAX precursor. These findings from this project agrees with result obtained by Frey et al. as well as result from literature, which proves the robustness of my model. However, future work could be done to experimentally synthesize the predicted MXene in order to further prove the reliability of my model.

References

[1] K. Hantanasirisakul et al. “Fabrication of Ti3C2Tx MXene Transparent Thin Films with Tunable Optoelectronic Properties”. In: *Advanced Electronic Materials* 2.6 (2016), pp. 1–7. ISSN: 2199160X. DOI: 10.1002/aelm.201600050.

[2] X. Jin et al. “Flame-retardant poly(vinyl alcohol)/MXene multilayered films with outstanding electromagnetic interference shielding and thermal conductive performances”. In: *Chemical Engineering Journal* 380.July 2019 (2020), p. 122475. ISSN: 13858947. DOI: 10.1016/j.cej.2019.122475. URL: https://doi.org/10.1016/j.cej.2019.122475.

[3] L. He et al. “Large-scale production of simultaneously exfoliated and Functionalized Mxenes as promising flame retardant for polyurethane”. In: *Composites Part B: Engineering* 179 (2019), p. 107486. ISSN: 1359-8368. DOI: https://doi.org/10.1016/j.compositesb.2019.107486. URL: http://www.sciencedirect.com/science/article/pii/S1359836819324023.

[4] H. Huang et al. “Synergistic effect of MXene on the flame retardancy and thermal degradation of intumescent flame retardant biodegradable poly (lactic acid) composites”. In: *Chinese Journal of Chemical Engineering* 28.7 (2020), pp. 1981–1993. ISSN: 1004-9541. DOI: https://doi.org/10.1016/j.cjche.2020.04.014.

[5] F. Shahzad et al. “Electromagnetic interference shielding with 2D transition metal carbides (MXenes)”. In: *Science* 353.6304 (2016), pp. 1137–1140. ISSN: 10959203. DOI: 10.1126/science.aag2421.

[6] G. Choi et al. “Enhanced Terahertz Shielding of MXenes with Nano-Metamaterials”. In: *Advanced Optical Materials* 6.5 (2018), pp. 1–6. ISSN: 21951071. DOI: 10.1002/adom.201701076.

[7] B. Akuzum et al. “Rheological Characteristics of 2D Titanium Carbide (MXene) Dispersions: A Guide for Processing MXenes”. In: *ACS Nano* 12.3 (2018), pp. 2685–2694. ISSN: 1936086X. DOI: 10.1021/acsnano.7b08889.

[8] K. Maleski, V. N. Mochalin, and Y. Gogotsi. “Dispersions of Two-Dimensional Titanium Carbide MXene in Organic Solvents”. In: *Chemistry of Materials* 29.4 (2017), pp. 1632–1640. ISSN: 15205002. DOI: 10.1021/acs.chemmater.6b04830.

[9] M. Naguib et al. “MXene: a promising transition metal carbide anode for lithium-ion batteries”. In: *Electrochemistry Communications* 16.1 (2012), pp. 61–64. ISSN: 1388-2481. DOI: https://doi.org/10.1016/j.elecom.2012.01.002.

[10] X. Jiang et al. “Inkjet-printed MXene micro-scale devices for integrated broadband ultrafast photonics”. In: *npj 2D Materials and Applications* 3.1 (2019). ISSN: 23977132. DOI: 10.1038/s41699-019-0117-3. URL: http://dx.doi.org/10.1038/s41699-019-0117-3.

[11] A. Sarycheva et al. “2D titanium carbide (MXene) for wireless communication”. In: *Science Advances* 4.9 (2018), pp. 1–9. ISSN: 23752548. DOI: 10.1126/sciadv.aau0920.

[12] J. Halim et al. “Transparent conductive two-dimensional titanium carbide epitaxial thin films”. In: *Chemistry of Materials* 26.7 (2014), pp. 2374–2381. ISSN: 15205002. DOI: 10.1021/cm500641a.

[13] X. Tang et al. “Engineering Aggregation-Resistant MXene Nanosheets As Highly Conductive and Stable Inks for All-Printed Electronics”. In: *Advanced Functional Materials* 2010897 (2021), p. 2010897. ISSN: 1616-301X. DOI: 10.1002/adfm.202010897.

[14] M. Naguib et al. “Two-dimensional nanocrystals produced by exfoliation of Ti 3AlC 2”. In: *Advanced Materials* 23.37 (2011), pp. 4248–4253. ISSN: 09359648. DOI: 10.1002/adma.201102306.

[15] J. L. Hart et al. “Control of MXenes’ electronic properties through termination and intercalation”. In: *Nature Communications* 10.1 (2019). ISSN: 20411723. DOI: 10.1038/s41467-018-08169-8. URL: http://dx.doi.org/10.1038/s41467-018-08169-8.

[16] Y. Lee et al. “Oxidation-resistant titanium carbide MXene films”. In: *Journal of Materials Chemistry A* 8.2 (2020), pp. 573–581. ISSN: 20507496. DOI: 10.1039/c9ta07036b.

[17] Z. Fan et al. “A nanoporous MXene film enables flexible supercapacitors with high energy storage”. In: *Nanoscale* 10.20 (2018), pp. 9642–9652. ISSN: 2040-3364. DOI: 10.1039/C8NR01550C.

[18] N. C. Frey et al. “Prediction of Synthesis of 2D Metal Carbides and Nitrides (MXenes) and Their Precursors with Positive and Unlabeled Machine Learning”. In: *ACS Nano* 13.3 (2019), pp. 3031–3041. ISSN: 1936086X. DOI: 10.1021/acsnano.8b08014.

[19] M. Naguib et al. “25th anniversary article: MXenes: A new family of two-dimensional materials”. In: *Advanced Materials* 26.7 (2014), pp. 992–1005. ISSN: 09359648. DOI: 10.1002/adma.201304138.

[20] M. He and L. Zhang. “Machine learning and symbolic regression investigation on stability of MXene materials”. In: *Computational Materials Science* 196.April (2021). ISSN: 09270256. DOI: 10.1016/j.commatsci.2021.110578.

[21] A. C. Rajan et al. “Machine-learning-assisted accurate band gap predictions of functionalized mxene”. In: *Chemistry of Materials* 30.12 (2018), pp. 4031–4038. ISSN: 15205002. DOI: 10.1021/acs.chemmater.8b00686.

[22] M. Khazaei et al. “Novel electronic and magnetic properties of two-dimensional transition metal carbides and nitrides”. In: *Advanced Functional Materials* 23.17 (2013), pp. 2185–2192. ISSN: 1616301X. DOI: 10.1002/adfm.201202502.

[23] M. Alhabeb et al. “Guidelines for Synthesis and Processing of Two-Dimensional Titanium Carbide (Ti 3 C 2 T”. In: (2017). DOI: 10.1021/acs.chemmater.7b02847.

[24] B. Anasori, M. R. Lukatskaya, and Y. Gogotsi. *2D metal carbides and nitrides (MXenes)*. Vol. 2. 2. 2017. ISBN: 9783030190255. DOI: 10.1038/natrevmats.2016.98.